Renewable Energy 65 (2014) 192–201

Contents lists available at ScienceDirect

Renewable Energy

journal homepage: www.elsevier.com/locate/renene

Numerical simulation of flatback airfoil aerodynamic noise

Taehyung Kim [a], Minu Jeon [a], Soogab Lee [a, b], Hyungki Shin [c, *]

[a] Department of Mechanical and Aerospace Engineering, Seoul National University, 1 Gwanak-ro, Gwanak-gu, Seoul 151-742, South Korea
[b] Institute of Advanced Aerospace Technology, Department of Mechanical and Aerospace Engineering, Seoul National University, 1 Gwanak-ro, Gwanak-gu, Seoul 151-742, South Korea
[c] Energy Efficiency Department, Korea Institute of Energy Research, 152 Gajeong-ro, Yuseong-gu, Daejeon 305-343, South Korea

ARTICLE INFO

Article history:
Received 21 February 2013
Accepted 23 August 2013
Available online 17 September 2013

Keywords:
Large wind turbine
Flatback airfoil
Root blade
Aerodynamic noise

ABSTRACT

The present paper presents a possible path for developing a large eddy simulation (LES) applicable to high Reynolds-number complex turbulent flows and the performance of the coupling of LES with statistical turbulence models around the flow over a blunt trailing edge configuration. The turbulent fluctuations in the boundary layers at the inflow region of the LES domain are generated by a synthesized turbulence method. The hybrid RANS-LES model showed considerable improvement in prediction accuracy even at a moderate grid resolution. The aerodynamic comparison with experimental data shows like results for the pressure distributions surrounding a flatback airfoil. To predict accurately the noise radiation from the blunt trailing edge and to save computational costs, the near-field region is computed by embedded LES while the surrounding region is simultaneously computed by RANS. The Brooks, Pope, and Marcolini (BPM) semi-empirical model is used for noise comparison with the hybrid RANS-LES result and experimental data. The present hybrid RANS-LES method is found to be adequate for predicting aerodynamic noise generation by vortical flow in the vicinity of a blunt trailing edge airfoil over a range of frequencies.

1. Introduction

The inboard region of large wind turbine blades requires thick airfoils to meet structural requirements. The use of flatback airfoils permits the use of airfoils of increased thickness without the chord increases that would occur if thick conventional airfoils were used. Avoiding this additional chord length makes the resulting structural design more compact and easier to construct, resulting in a blade that can be more easily transported [1]. Despite their numerous benefits, including the aforementioned structural improvements, high sectional lift coefficients and a reduction of sensitivity to leading edge surface soiling, flatback airfoils also induce increased blade drag and trailing edge vortex shedding noise. Due to their high Reynolds number, the wake of flatback airfoils is accompanied by three-dimensional instabilities which emerge as pairs of counter-rotating streamwise vortices. These three-dimensional instabilities are dependent on the airfoil's Reynolds number, free stream turbulence and the turbulent layer boundaries at the two ends of the three-dimensional blunt trailing edge of the profiled body [2].

Large eddy simulation (LES) is well known as a useful tool to predict practical turbulence problems. Although LES needs far fewer grid nodes than direct numerical simulation (DNS), there still remain several serious difficulties in its application to high Reynolds-number flows. In LES, only the dissipative scales of turbulence, which are assumed to have a more isotropic character than the large scales in a shear-driven flow, are modeled while the eddies carrying the bulk of the energy of the flow are resolved. However, in the near-wall region, the number of grid points increases drastically because the temporal and spatial scales of the energy-containing eddies become very small. Therefore, LES cannot be applied to large-scale flow problems.

To overcome these difficulties, a hybrid RANS/LES model originally based on the concept of a hybrid model connecting LES with Reynolds-Averaged Navier-Stokes (RANS) modeling in the near-wall region has emerged. A number of researchers have explored this concept (Davidson et al. [3], Hanjalic et al. [4], Temmerman et al. [5], Kenichi Abe et al. [6]) with positive results encouraging further development of this field. On the other hand, very few studies have included a detailed description of the near-wall

* Corresponding author. Tel.: +82 42 860 3748; fax: +82 42 860 3133.
E-mail addresses: zestriver@snu.ac.kr (T. Kim), ace55@snu.ac.kr (M. Jeon), solee@snu.ac.kr (S. Lee), hkeewind@kier.re.kr (H. Shin).

0960-1481/$ – see front matter © 2013 Elsevier Ltd. All rights reserved.
http://dx.doi.org/10.1016/j.renene.2013.08.036

turbulence and acoustic prediction when the hybrid RANS/LES models are applied to flow and noise predictions.

Segregated modeling stands in contrast to methods of unified modeling such as RANS, LES, and DNS. In the segregated modeling, LES is employed in one part of the computational domain while RANS is used in the remainder [7]. The resolved quantities are no longer continuous at the RANS/LES interfaces. Instead, LES and RANS computations are performed nearly independently in their respective sub-domains. The computed results are then matched through appropriate boundary conditions. The embedded LES method is a type of segregated modeling and is composed of full two-way coupling between the RANS and LES zones. The LES-inflow boundary of an LES embedded in a RANS solution is assumed to be steady. The steady RANS solution does not provide any turbulence fluctuations. Performing LES on the downstream side of the RANS interface requires proper LES-boundary conditions.

The aerodynamic and acoustic optimization process with the prediction of noise generation can be found in studies on various airfoils conducted by Kim et al. [8] and Göçmen et al. [9]. These studies are based on geometrical approaches around the pressure side, suction side, and the trailing edge of sharp airfoils used on small-scale wind turbines. The measured and predicted directivity in the far field for a wind turbine from Ref. [10] showed that there is an apparent directivity for the total noise of a wind turbine where there is lower sound levels in the crosswind direction compared to other points around the wind turbine with equal distance from the source. The horizontal directivity pattern is of a dipole character due to the fat that the emitted sound from the dominant sound source is decreased in the crosswind direction. The aerodynamic sources which are also of a dipole character along the blade's airfoil in the vertical plane constitute the directivity in the vertical plane as well as the horizontal.

For the inboard region of rotating blades which have flatback airfoils, the velocities and corresponding Reynolds numbers are much lower than the outboard region of blades. However, the use of flatback airfoils for the inboard region of wind turbine blades can increase aerodynamic noise because the blunt trailing edged airfoil has nearly omni-directional noise directivity and quasi-tonal noise characteristics [11]. Therefore, the blunt vortex shedding noise can be dominant in the crosswind direction while the trailing edge noise is decreased due to its dipole characteristics.

The present paper is a contribution to the ongoing research to create a better turbulence model applicable to complex turbulent flows and the aeroacoustic prediction of flatback airfoils used in large wind turbines at moderate computational cost. Aerodynamic measurements were made in these experiments for comparison with computational results. The Brooks, Pope, and Marcolini (BPM) semi-empirical model [11] is used for noise comparison with the hybrid RANS-LES result and experimental data. The noise predictions related to flatback airfoils used in large wind turbines were obtained using a hybrid RANS-LES method and the Ffowcs Williams–Hawkings equation [12].

2. Methods and test cases

The hybrid RANS-LES model is used to predict the aerodynamic performance of sharp and flatback airfoils by the CFD solver Fluent [13]. The hybrid RANS-LES methods are based on decomposing the entire domain into clearly identifiable regions for RANS and LES before starting the simulation. The connection between the distinct zones during the simulation is established via explicit coupling of the solution, i.e. velocities and pressure, at the interfaces. The hybrid RANS-LES model concepts and boundary layer conditions used in this study are shown in Fig. 1.

The most critical interface is the interface where the flow leaves the RANS domain and enters the LES region (RANS/LES interface). At this interface, it is necessary to convert modeled turbulence kinetic energy into resolved energy for this transfer using an appropriate method. Synthetic turbulent fluctuations are obtained by two methods: the random vortex method and the synthesized turbulence method.

The noise prediction is performed by the Ffowcs Williams–Hawkings equation, which is extended from Lighthill's acoustic analogy. The hybrid RANS-LES model provides the acoustic pressure signal at the observer's location. The Brooks, Pope, and Marcolini (BPM) semi-empirical model is used for the prediction of the self-noise produced by the sharp and flatback airfoils. The numerical models contain three main sources of airfoil self-noise: turbulence boundary layer trailing edge noise, laminar boundary layer vortex shedding noise, and blunt trailing edge vortex shedding noise. This study does not take into account the turbulent inflow noise prediction method developed by Amiet et al. [14] because this noise is more sensitive to natural atmospheric and terrain conditions than airfoil geometry.

2.1. Hybrid RANS-LES interface treatments

2.1.1. The random vortex method

This is the most common fluctuation generation method for RANS/LES interfaces to convert modeled turbulence kinetic energy into resolved energy. Based on studies done by Mathey et al. [15], a perturbation is added to a specified mean velocity profile via a fluctuating vorticity field. The vortex method is based on the Lagrangian form of the 2D evolution equation. These particles, or "vortex points", are converted randomly and carry information about the vorticity field.

The resulting scaling model to generate turbulence fluctuation for the RANS-LES interface is then:

$$u_i'^{*} = u_i' \frac{\sqrt{\langle u_i u_i \rangle}}{2/3k} \tag{1}$$

where $u_i'^{*}$ and u' are the scaled and unscaled velocity fluctuations respectively. Other parameters in Eq. (1) above are k, the turbulent kinetic energy; and $\langle u_i u_i \rangle$, the normal statistic velocity fluctuations.

2.1.2. The synthesized turbulence method

One commonly-used method for generating turbulent inlets is to synthesize them according to particular constraints [16]. In this method, turbulence is analyzed by decomposition onto a basis set of harmonic functions to easily perform Fourier analysis. The

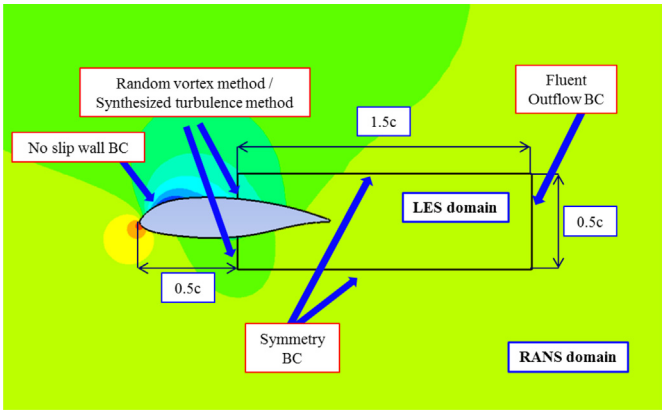

Fig. 1. The hybrid LES/RANS model and boundary layer conditions.

turbulent fluctuations are represented by a linear sum of sine and cosine functions, with coefficients representing the energy contained in each mode. The final instantaneous flow profile is composed of the mean velocity profile and the generated arbitrary fluctuating profile.

$$u_x(y,t) = \overline{u}_x(y) + u'_x(y,t) = \overline{u}_x(y) + u_m \sum_{i=1}^{N} a'_i(t)\cos\left(i\kappa y + \varphi'_i(t)\right) \tag{2}$$

here u_x is the x-component of the instantaneous velocity, and y is a coordinate across the inlet to the domain. $a'_i(t)$ and $\varphi'_i(t)$ are coefficients to be determined from some form of a constrained random process. $i\kappa$ is the wave number.

2.2. The Ffowcs Williams and Hawkings equation

For an airfoil, the aerodynamic sound generation by turbulence and surfaces in arbitrary motion can be predicted by Williams and Hawkings equation [12] which is based on Lighthill's acoustic analogy [17]. This is the rearranged Navier–Stokes equation which has the form of an inhomogeneous wave equation with a quadrupole source distribution in the volume surrounding the body and monopole and dipole sources on the body surface. The differential form of the Ffowcs Williams–Hawkings (FW–H) equation can be described as:

$$\frac{1}{c^2}\frac{\partial^2}{\partial t^2}p'(\vec{x},t) - \nabla^2 p'(\vec{x},t) = \frac{\overline{\partial}}{\partial t}\left[\rho_0 v_n \delta(f)\right] - \frac{\overline{\partial}}{\partial x_i}\left[l_i\delta(f)\right] + \frac{\overline{\partial}^2}{\partial x_i \partial x_j}\left[T_{ij}H(f)\right] \tag{3}$$

where v_n is the local velocity of the body in the direction normal to the surface defined by $f = 0$, l_i are the components of the local force on the surface, and $\delta(f)$ and $H(f)$ are the Dirac delta and Heaviside functions respectively.

The first and second terms in RHS are the monopole source and the dipole source respectively. Both sources have surface source characteristics. The third term is a quadrupole source term that acts throughout the volume that is exterior to the body surface. The monopole or thickness source term models the noise generated by the displacement of fluid as the body passes through it. The dipole or loading source term models the noise that results from the unsteady motion of the force distribution on the body surface. The quadrupole source term models the non-linearities due to both the local sound speed variation and the finite fluid velocity near the body surface. This source is considerable only in transonic or supersonic conditions. In this study, the prediction of volume noise source is neglected because the wind turbine blades are operated in the low Mach number flow field.

The speed and accuracy of the noise calculation is improved by eliminating the time derivative of the first integral in Farassat formulation 1A [18,19]:

$$p'(\vec{x},t) = p'_T(\vec{x},t) + p'_L(\vec{x},t) \tag{4}$$

where

$$4\pi p'_T(\vec{x},t) = \int_{f=0}\left[\frac{\rho_0(\dot{v}_n + v_{\dot{n}})}{r|1-M_r|^2}\right]_{\text{ret}} \mathrm{d}S + \int_{f=0}\left[\frac{\rho_0 v_n\left(r\dot{M}_r + cM_r - cM^2\right)}{r^2|1-M_r|^3}\right]_{\text{ret}} \mathrm{d}S \tag{5}$$

$$4\pi p'_L(\vec{x},t) = \frac{1}{c}\int_{f=0}\left[\frac{\dot{l}_r}{r|1-M_r|^2}\right]_{\text{ret}} \mathrm{d}S + \int_{f=0}\left[\frac{l_r - l_M}{r|1-M_r|^2}\right]_{\text{ret}} \mathrm{d}S + \frac{1}{c}\int_{f=0}\left[\frac{l_r\left(r\dot{M}_r + cM_r - cM^2\right)}{r^2|1-M_r|^3}\right]_{\text{ret}} \mathrm{d}S \tag{6}$$

In this formulation, integrands with $1/r$ are far-field terms and those with $1/r^2$ are near-field terms. A dot over a variable indicates the source time derivative of that variable. The subscript n, r and M refer to the dot product with the unit normal vector, the unit radiation vector, and the surface velocity vector normalized by the speed of sound, respectively.

2.3. Semi-empirical noise models

2.3.1. Turbulent boundary layer trailing edge noise

This noise is the most common airfoil self-noise source especially for high Reynolds number flows. The turbulent boundary layer trailing edge noise is caused by the interaction between boundary layer turbulence and the blade's trailing edge. It has broadband nature and this noise is a primary source of high-frequency noise. The turbulent boundary layer trailing edge noise is modeled as the combination of the pressure side noise, the suction side noise and the separation noise by Brooks et al. [11]

$$\mathrm{SPL}_{\text{total}} = 10\log\left(10^{\mathrm{SPL}_p/10} + 10^{\mathrm{SPL}_s/10} + 10^{\mathrm{SPL}_\alpha/10}\right) \tag{7}$$

$$\mathrm{SPL}_p = 10\log\left(\frac{\delta_p^* M^5 L \overline{D}_h}{r_e^2}\right) + A\left(\frac{\mathrm{St}_p}{\mathrm{St}_1}\right) + (K_1 - 3) + \Delta K_1 \tag{8}$$

$$\mathrm{SPL}_s = 10\log\left(\frac{\delta_s^* M^5 L \overline{D}_h}{r_e^2}\right) + A\left(\frac{\mathrm{St}_s}{\mathrm{St}_1}\right) + (K_1 - 3) \tag{9}$$

$$\mathrm{SPL}_\alpha = 10\log\left(\frac{\delta_s^* M^5 L \overline{D}_h}{r_e^2}\right) + B\left(\frac{\mathrm{St}_s}{\mathrm{St}_2}\right) + K_2 \tag{10}$$

In the above equations, δ_p^* and δ_s^* are the boundary layer displacement thickness for the pressure side and suction side respectively. Other parameters in Eqs. (8)–(10) are M, the Mach number; L, the airfoil span length; r_e, the effective observer distance; A and B, the empirical spectral shape functions based on the Strouhal number; K_1 and K_2, the amplitude functions based on α_*, the effective aerodynamic angle of attack, and Re_c, the Reynolds number based on the chord length; and $\overline{D}_h$ is the directivity function for high-frequency noise.

2.3.2. Blunt trailing edge vortex shedding noise

This noise is caused by vortex sheddings from the blunt trailing edge. The efficient tonal noise is radiated from the trailing edge. The sharpening of the trailing edge will shift the noise peak towards the ultrasound region. However, the flatback airfoil inherently possesses blunt trailing edge noise sources because of the thick trailing edge. The blunt trailing edge vortex shedding noise is described as:

$$\mathrm{SPL}_{\mathrm{blunt}} = 10\log\left(\frac{hM^{5.5}\Delta L\overline{D}_h}{r^2}\right) + G_4\left(\frac{h}{\delta^*_{\mathrm{avg}}}, \Psi\right) + G_5\left(\frac{h}{\delta^*_{\mathrm{avg}}}, \Psi, \frac{\mathrm{St}'''}{\mathrm{St}'''_{\mathrm{peak}}}\right) \quad (11)$$

where h is the trailing edge thickness and δ^*_{avg} is the average boundary layer displacement thickness for pressure and suction sides of the flatback airfoil. Ψ is the solid angle, in degree, between the sloping surfaces upstream of the trailing edge. G_4 is the function to determine the peak level of the spectrum and G_5 is the function to define the shape of the spectrum. St‴ is the Strouhal number, defined as $\mathrm{St}''' = fh/U$. $\overline{D}_h$ is the high frequency directivity function defined as:

$$\overline{D}_h(\Theta_e, \Phi_e) \approx \frac{2\sin^2(\Theta_e/2)\sin^2\Phi_e}{(1 + M\cos\Theta_e)[1 + (M - M_e)\cos\Theta_e]^2} \quad (12)$$

where the overbar on $\overline{D}_h$ indicates that it is normalized by the trailing edge noise radiated normal to the streamwise axis ($\Theta_e = 90°$) and the flyover plane ($\Phi_e = 90°$) direction.

2.4. Test cases and computational conditions

The test flatback airfoils are categorized into two groups. The first airfoil group is composed of DU97-W-300 and DU97-flatback airfoils, which is tested for aeroacoustic characteristics. The second airfoil group contains KWA029-400 which is based on the DU00-W2-401 airfoil. This airfoil is tested for the similarities and differences in aerodynamic performance between different numerical approaches and experiments. The numerical approaches are the XFOIL panel method, RANS, LES, and hybrid RANS-LES methods.

The blunt trailing edge profiled body geometry for the numerical model for the first airfoil group, which has a thickness-to-chord ratio of $t/c = 12.5$, is similar to that studied by Barone et al. [20]. The baseline airfoil TU-Delft DU97-W-300 has a sharp trailing edge thickness of $t/c = 1.7$, while the modified airfoil TU-Delft DU97-flatback has a blunt trailing edge thickness of $t/c = 10$, as shown in Fig. 2. The chord length of the profiled body in the numerical solution is $c = 0.91$ m. The numerical simulations are carried at $Re_c = 3{,}000{,}000$ for an angle of attack 4°.

The solution domain is defined as a tetrahedral volume surrounding the profiled body. The domain extends 10c behind, 10c in front of, and 10c above and below the upper and lower surfaces of the body. The region surrounding the solid walls of the body is discretized using a boundary layer-type structured grid of hexahedral cells, which are refined towards the wing surfaces. The remaining part of the solution domain, which encompasses the inner region, is discretized using an unstructured grid of tetrahedral cells. The grid size has been previously increased in steps of +9%. The close up views of the final hybrid grids, which has

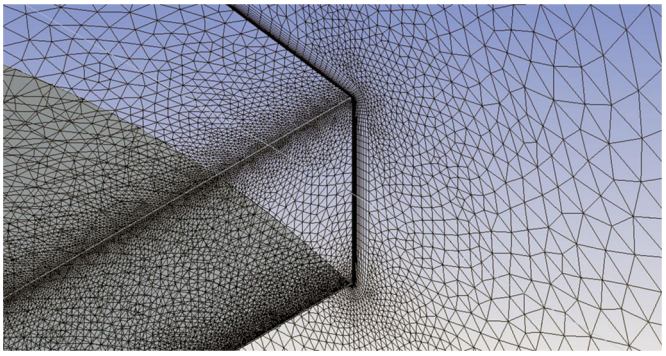

Fig. 3. Close-up view of the mesh near the DU97-flatback airfoil trailing edge.

2.9×10^5 cells for RANS domain and 3.9×10^6 cells for LES domain, are shown in Fig. 3 for the DU97-flatback airfoil. The numerical solutions are validated by tests performed in the Virginia Tech Stability Wind Tunnel, a continuous, single-return, subsonic wind tunnel with a 1.83-m (6-ft) square, 7.3-m (24-ft) long removable rectangular test section. Details of the numerical solution procedure are provided in Berg et al. [21].

The second flatback airfoil body geometry used for the numerical model and experimental model is KWA029-400, the test model developed by the Korea Institute of Energy Research (KIER) based on the DU00-W2-401 airfoil (Fig. 4). As it is not shown here, the experimental facility has a long, constant rectangular cross-section duct 1.25 m high and 1.249 m wide, resulting in a fully-developed turbulent flow at the end of the inlet rectangular duct. The Reynolds number is 1×10^6 based on the airfoil chord length and the bulk-mean inflow velocity. The chord length of the flatback airfoil body is 0.35 m. The test angle of attack is 0°. The unstructured mesh for the computational domain and refined region surrounding the KWA029-400 airfoil are shown in Fig. 5. The segregated implicit scheme based on the SIMPLE algorithm from Fluent has been used to calculate the governing equations in three dimensions. Temporal discretization is performed using a time step size of 1.0×10^{-5} s.

2.5. Test facility, models and test methodology

The KIER aerodynamic tests in this work were performed in the Chungnam National University anechoic wind tunnel. The facility was capable of acquiring aerodynamic loads on the test airfoil (through the use of airfoil surface pressure ports and a wake rake), detailed hot-wire measurements in the trailing edge boundary layer and detailed acoustic source data. The test section size was 1.250 m × 1.250 m and the maximum velocity was 70 m/s.

The airfoil model used in this test was composed of aluminum alloy. This model was 0.35 m in chord and 1.249 m in span. The 11%

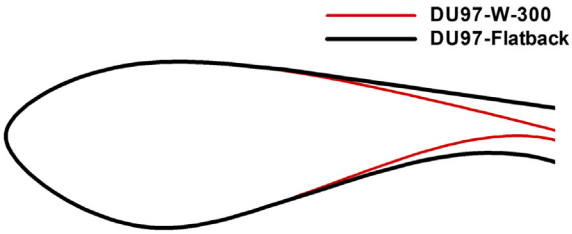

Fig. 2. Airfoil geometry comparison (DU97-W-300 and flatback).

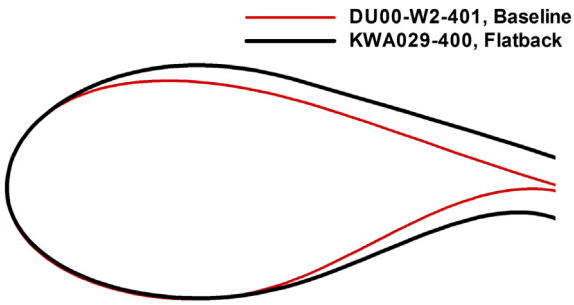

Fig. 4. Airfoil geometry comparison (DU00-W2-401 and KWA029-400).

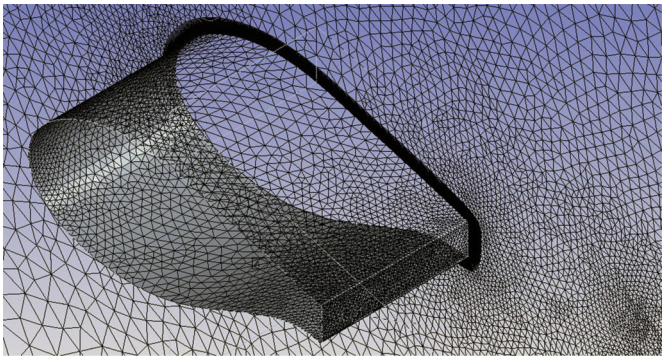

Fig. 5. The unstructured mesh for the computational domain and refined region surrounding the KWA029-400 airfoil.

flatback trailing edge was 3.85 cm thick. The model was inserted through the floor of the test section and was mounted vertically, as illustrated in Fig. 6. The three-axis balance treatment and calibration were performed for the accurate measurements of lift, drag and pitching moment.

The blockage ratio was kept smaller than 5% to avoid blockage effect. All measurements were obtained with the airfoil stationary. The model angle of attack was set, the tunnel operating speed was brought up to the appropriate levels for the Reynolds numbers of interest and the required measurements were obtained at each Reynolds number.

Turbulent boundary layer trailing edge noise is generally considered to be the most important source of airfoil self-noise for modern wind turbine blades. In this phenomenon, the unsteady pressure waves in the turbulent boundary layer are amplified and radiated by the trailing edge. As the angle of attack increase, the thickness of the turbulent boundary layer increases and large-scale unsteady structures can dominate noise production from the trailing edge. For fully separated flow, noise can radiate from the entire chord [22].

Laminar boundary layer vortex shedding noise is not likely to be important for large wind turbines operating at high Reynolds number, but it may be significant for small wind turbines. Therefore, The fully developed boundary layer condition was used for experiments. For tests with a fully turbulent boundary layer, tripping was initiated using zigzag tape of with = 5% chord over the entire model span at 2% and 5% chord on the suction and pressure sides of the airfoil, respectively. The trip thickness was 0.25 mm.

The pressures from the model surface taps were measured with a Pressure scanner system with LabVIEW 7.1 of National Instrument. Wake pressures were measured with a single Pitot static probe mounted on a traversing mechanism near the airfoils mid span. All pressure measurements were 1-s averages of data acquired at 1000 Hz through the 50 pressure hole taps on the airfoil surface. The pressure sensors were composed of MPX5010 and MPX5050 for maximum pressure 10 kPa and 50 kPa, respectively.

3. Results and discussion

3.1. Aerodynamic results

For judging convergence, the onset of transition for the suction and pressure sides was estimated per 1000 iterations. The

Fig. 6. The KIER aerodynamic tests in the Chungnam National University anechoic wind tunnel (upper; test section, lower; pressure tap sensors).

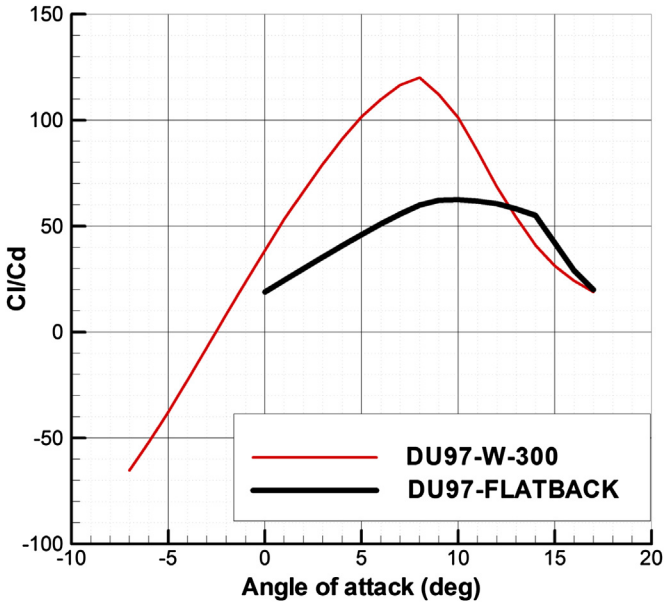

Fig. 7. Lift to drag ratios for DU97-W-300 and DU97-flatback ($Re_c = 3 \times 10^6$).

computation stops when the invariance on the transition location is found in the iterative process, i.e. when transition location change falls within 1% chord. After that, the Fluent run is continued until default convergence criteria in ANSYS Fluent on variable residuals and global force coefficients are satisfied.

The XFOIL program [23] has been used to analyze and compare the primary aerodynamic performance parameter which is the ratio of lift coefficient, C_L, and drag coefficient, C_D, according to the angle of attack, α and the results are shown graphically in Figs. 7 and 8.

The maximum lift to drag ratio has been decreased from 120 to 65 for the DU97-flatback airfoil in Fig. 7. This result means that an overall aerodynamic performance is lowered when the flatback airfoil is generated by opening up the trailing edge of the airfoil with preserving the camber line of the original airfoil. The lift to

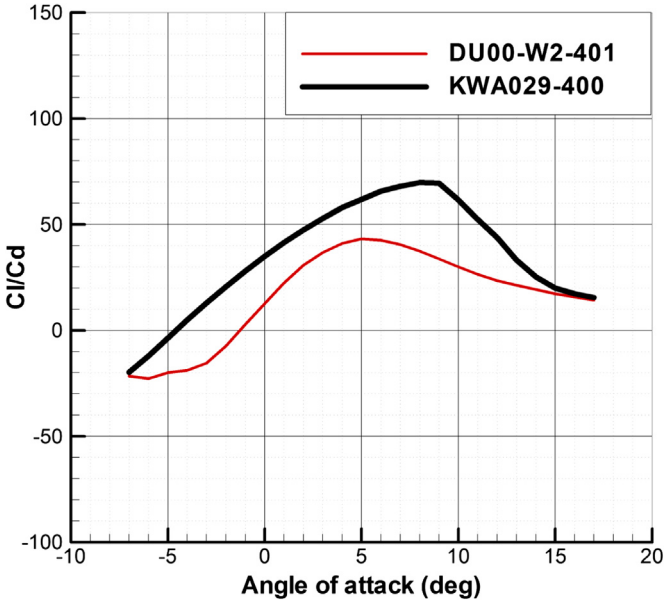

Fig. 8. Lift to drag ratios for DU00-W2-401 and modified KWA029-400 ($Re_c = 1 \times 10^6$).

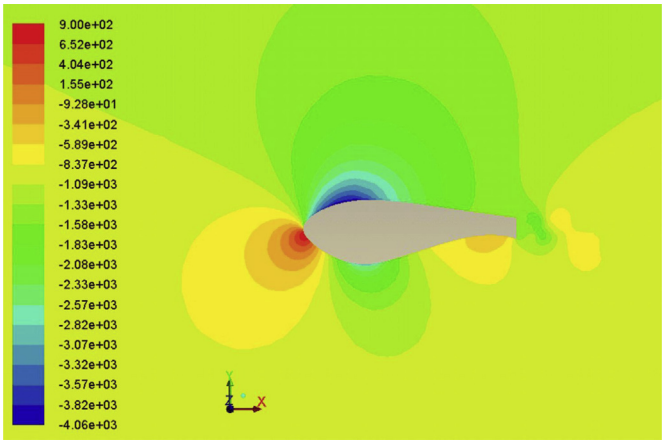

Fig. 9. The pressure distribution surrounding the DU97-flatback airfoil ($Re_c = 3 \times 10^6$ at $\alpha = 4^\circ$).

drag ratios are slightly increased beyond the angle of attack 13°. However the result is not reliable after stall region because of the limit of XFOIL program.

As can be seen from Fig. 8, the maximum lift to drag ratio of the modified flatback version of DU00-W2-401, KWA029-400, is more than 70 where for DU00-W2-401 that value is slightly above 40. This result shows that the aerodynamic performance of a flatback version airfoil can be increased by a valuable optimization process with changing the camber line of the original airfoil.

Some illustrative results of the hybrid RANS-LES computations are shown below in Figs. 9 and 10, in which the contours of static pressures and velocities are plotted around the airfoil on the $z = 0$ plane. The wake patterns behind the airfoil clearly indicate the wake location and the presence of vortex structures near the trailing edge. The vorticity contours also provide clear pictures of the turbulence which convects past the blunt trailing edge in Fig. 11 for the hybrid RANS-LES method and in Fig. 12 for the full LES, respectively. In the following sections, both aerodynamic and aeroacoustic results from the RANS, LES, and hybrid RANS-LES simulations will be evaluated against the experimental data.

Quantitative comparisons of the airfoil's aerodynamic performance, in terms of pressure distributions, are shown in Fig. 13. The distribution of the pressure coefficient, defined as $C_p = 2(p-p_\infty)/\rho U^2{}_\infty$, is plotted alongside predictions from the XFOIL panel method

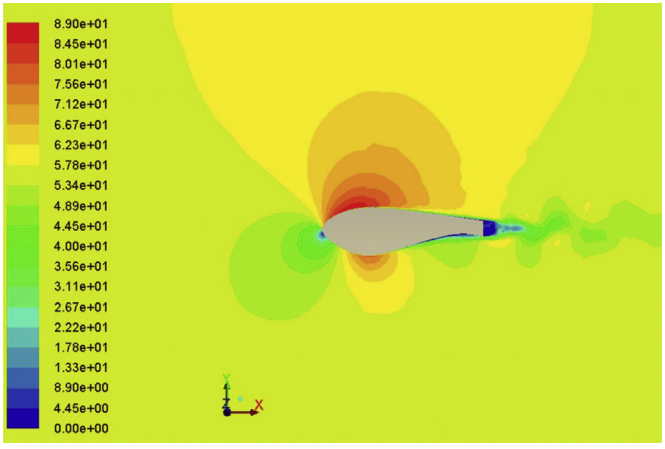

Fig. 10. The velocity field surrounding the DU97-flatback airfoil ($Re_c = 3 \times 10^6$ at $\alpha = 4^\circ$).

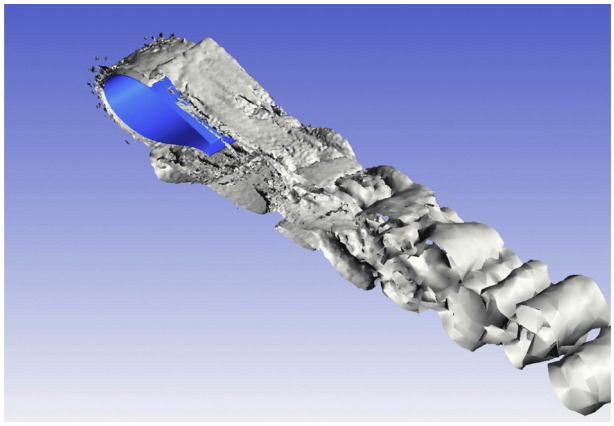

Fig. 11. Instantaneous snapshot of the fluid vorticity in the near-field domain computed by the hybrid RANS-LES ($Re_c = 3 \times 10^6$ at $\alpha = 4°$).

and experimental data from KIER. The *x*-axis represents the normalized chord length and the *y*-axis is the pressure coefficients. The XFOIL data shows over-predicted results on both the pressure and suction sides of the airfoil in the mid-chord region. For development of the fully turbulent flow, the XFOIL and the other CFD methods are computed under forced transition condition at the same transition locations as the KIER experiments. Therefore, the transition region in which the boundary layer flow changes from laminar to turbulent is not shown in this figure.

The result from the XFOIL data shows abrupt change of pressure coefficient at 60 percent of the chord. This result occurs on both upper and lower surfaces of the airfoil. This is due to the limitation of panel based method. XFOIL is basically developed for the aerodynamic performance prediction of various sharp airfoils which are used for aircrafts. For flatback airfoils, which have large trailing edge thickness, have strong wake vortex structures and also rotational flow characteristics near the trailing edges. Therefore, the panel-based XFOIL cannot predict aerodynamic characteristics accurately near the blunt trailing edges.

Pretty good agreements among the RANS, hybrid RANS-LES, LES, and the KIER experimental data are seen on both the pressure and suction sides of the airfoil. However, the RANS method shows some distorted results near blunt trailing edge, owing to limitations in the ability of the RANS method to compute high fluid vorticity near blunt trailing edges accurately. LES and Hybrid RANS-LES instantaneous wall-pressure distributions clearly show a turbulent flow

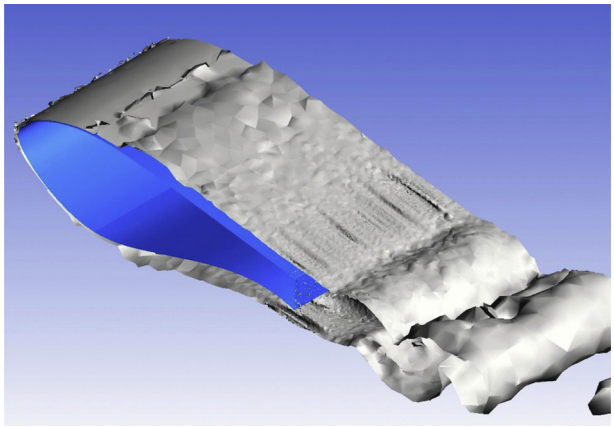

Fig. 12. Instantaneous snapshot of the fluid vorticity in the near-field domain computed by the full LES ($Re_c = 3 \times 10^6$ at $\alpha = 4°$).

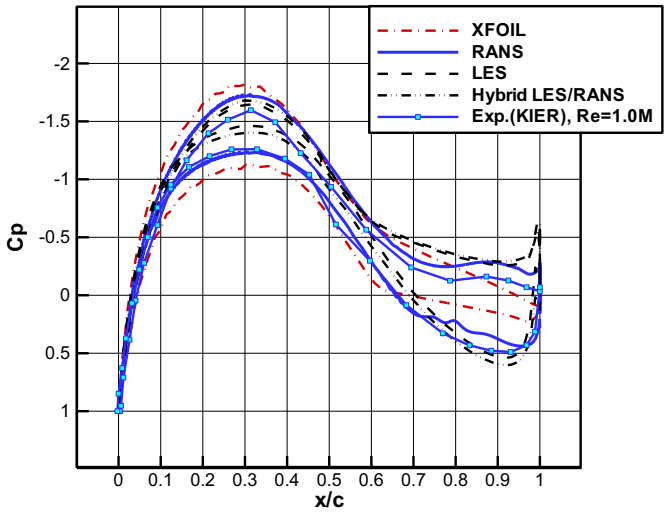

Fig. 13. A comparison of the pressure coefficient *Cp* between the XFOIL predictions, RANS simulation, LES simulation, hybrid LES/RANS simulation, and experimental data ($Re_c = 1 \times 10^6$ at $\alpha = 0°$).

condition with variations that can be traced to the instabilities of the turbulent boundary layers at the trailing edge.

3.2. Aero-acoustic results

The far-field acoustics from the semi-empirical calculations for the DU97-W-300 and DU97-flatback airfoils were compared against corresponding experimental data. For the far-field acoustics, the sound pressure levels (SPLs) were recorded in the prediction codes at the same observer locations as the Virginia Tech experiments. The experiments at Virginia Tech tested the DU97-W-300 airfoil and DU97-flatback airfoil with a chord length of 0.91 m, angle of attack of 4.0°, velocity of 56.5 m/s (Re = 3,000,000), and with a far-field measurement location that was situated on the mid−span plane, 3.12 m from the trailing edge and 112.0° from the streamwise axis.

Some convergence results of the hybrid RANS-LES computation are shown in Fig. 14. Noise prediction is calculated from $t = 0.07$ s after initial transients have been washed out as shown in Fig. 14 for drag and lift time history. These transients are emerged by the transition from RANS domain to LES domain at the RANS-LES interface because the coupled LES calculation is based on the previous RANS results.

The results of aero-acoustic comparisons for DU97-W-300 and DU97-flatback airfoils are shown in Fig. 15, which shows the predicted far-field noise by the hybrid RANS-LES computation at the same locations as in the experiments and with the same narrowband frequency averaging. It is obvious from these results that the flatback airfoil generates quasi-tonal noise than the original DU97-W-300 airfoil noise level at most frequencies.

For the hybrid RANS-LES computation for flatback airfoil, good agreement is seen in the peak frequencies (150−200 Hz) of the blunt trailing edge noise, and similar SPL rates of change at lower frequencies. Overall, the difference in SPL between numerical predictions and experimental measurements was within 10 dB for medium-to high-range frequencies.

The far-field acoustics from the semi-empirical calculation for the sharp and blunt airfoils were compared against corresponding experimental data in Fig. 16. The observer was located on the mid−span plane, 3.12 m from the trailing edge and 112.0° from the streamwise axis. In report [10] a semi-empirical prediction method

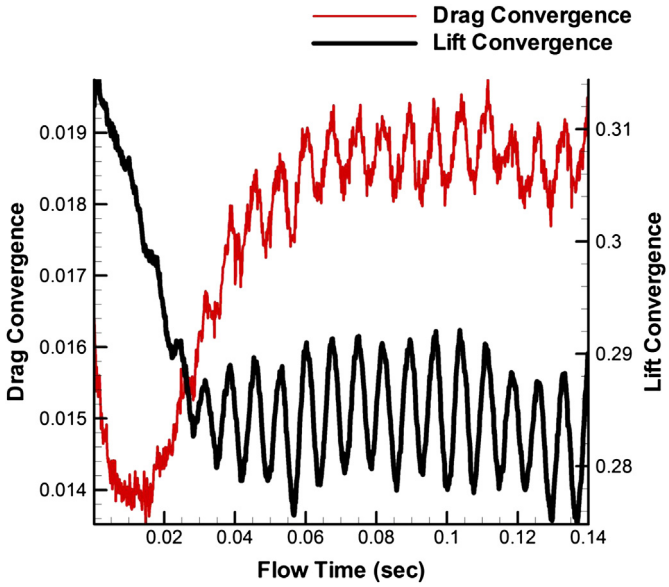

Fig. 14. Acoustic results of the hybrid LES/RANS simulation: drag and lift convergence time history ($Re_c = 3 \times 10^6$ at $\alpha = 4°$).

for trailing edge noise from wind turbines has been tested. The prediction code that needs the blade geometry and the turbine operating conditions was compared to measurements by an acoustic array and directivity measurements and the prediction showed the same characteristics as the results of the measurements. The report shows that noise that is emitted to the ground was produced when the blade of the rotor was moving downward. This is due to trailing edge noise directivity and convective amplification.

The numerical result for blunt trailing edged airfoil predicts significant noise emission near 100 Hz, while the peak frequency of the experiment is shown near 160 Hz. We find that the differences are caused by the limiting value of the peak Strouhal number of the

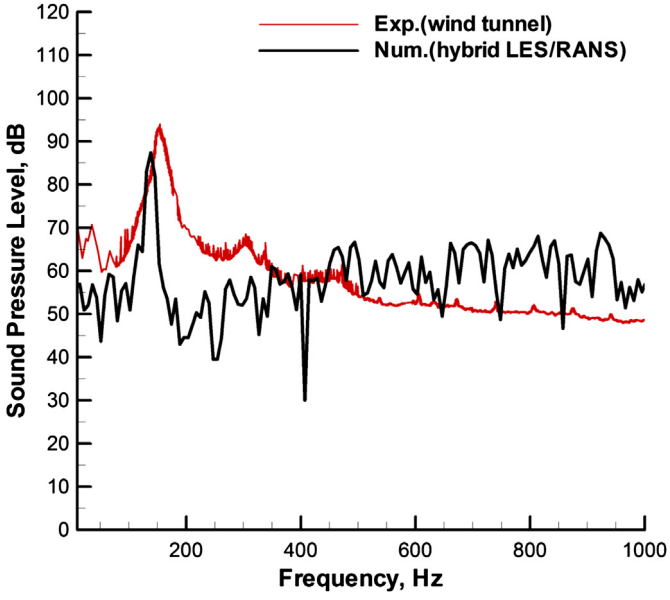

Fig. 15. A comparison of the far-field measurements obtained from the wind tunnel experiments along with the corresponding SPL calculated from the hybrid LES/RANS data for DU97-flatback ($Re_c = 3 \times 10^6$ at $\alpha = 4°$).

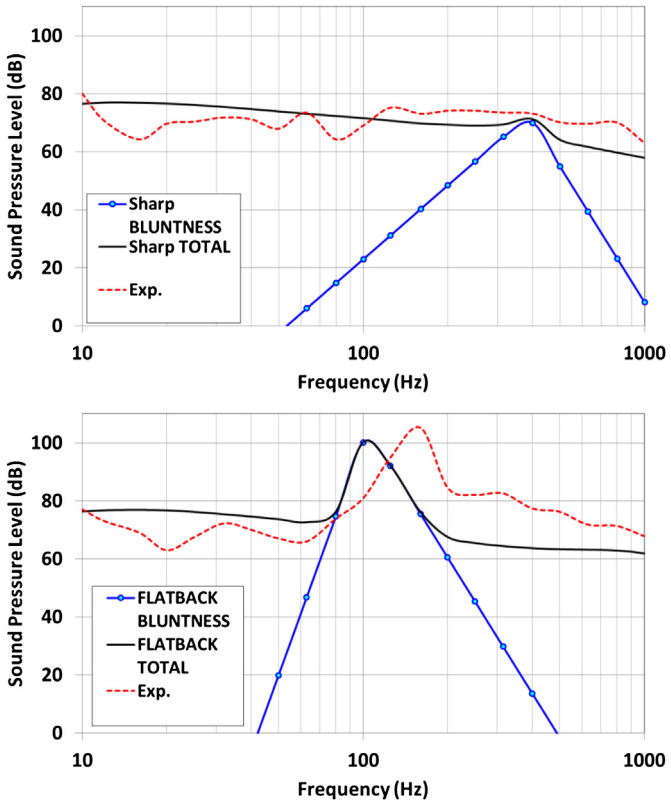

Fig. 16. A comparison of the far-field measurements obtained from the wind tunnel experiments along with the corresponding SPL calculated from the semi-empirical formula at the same observer position as the experiment for DU97-W-300 (upper; $Re_c = 3 \times 10^6$ at $\alpha = 4°$) and for DU97-flatback (lower; $Re_c = 3 \times 10^6$ at $\alpha = 4°$).

BPM model. The peak Strouhal numbers were 0.268 for experimental results and 0.2 for Blake's theory [24], respectively. The limiting values of thickness ratio h/δ^*_{avg}, defined as the ratio of trailing-edge thickness to the average boundary layer displacement thickness, were also beyond the maximum thickness ratio 10 of Blake's theory [24]. As expected from the previous discussion, the overall agreement of the sound pressure level shows that the hybrid RANS-LES method can be considered a promising concept for such high vorticity flow problems. The hybrid zonal approach is more accurate than the semi-empirical method.

4. Conclusion

LES, RANS, and hybrid RANS-LES have been carried out for turbulent boundary-layer flows past blunt trailing edges of several flatback airfoils at a chord Reynolds number of 1.0×10^6 and 3.0×10^6. The computed pressure distributions by LES and hybrid RANS-LES simulations compare more reasonably well with the experimental measurements of KIER than the results given by XFOIL and RANS computation. The discrepancies observed at some trailing edge stations may have been caused by inadequate inflow velocity conditions, a small computational spanwise domain size, or high vortex sheddings near the blunt trailing edge.

The far-field acoustics is computed from an integral form solution to the Lighthill equation developed by Ffowcs-Williams and Hawkings. The acoustic evaluation is performed in the Fourier frequency domain using source-field data obtained from the hybrid RANS-LES. To predict accurately the noise radiation from the blunt trailing edge and to save computational costs, the near-field region is computed by embedded LES and the surrounding region is computed by RANS

simultaneously. The space-time characteristics of surface pressure fluctuations are obtained to provide the acoustic source functions for the far-field noise calculation. The frequency spectra of surface pressure fluctuations obtained from the hybrid RANS-LES agree well with experimental measurements at the same observer location.

The present hybrid RANS-LES method is found to be adequate for predicting noise radiation over a range of frequencies compared to the BPM semi-empirical method. At the peak frequency and peak level of blunt trailing edge vortex shedding noise, however, the estimation based on surface pressure fluctuations does not precisely match the experimental measurements. This issue will be addressed in future simulations using an expanded computational domain and improved inflow velocity conditions.

Acknowledgment

This work was supported by the Human Resources Development Program (No. 20124030200030) and the New & Renewable Energy Technology Development Program (No. 20123010020130) of the Korea Institute of Energy Technology Evaluation and Planning (KETEP) grant funded by the Korea Government Ministry of Trade, Industry and Energy.

Nomenclature

Abbreviations

BPM	Brooks, Pope, and Marcolini
CFD	computational fluid dynamics
LES	large eddy simulation
SGS	subgrid scale
SIMPLE	semi-implicit method for pressure-linked equations
SPL	sound pressure level
SST	shear stress transport
RANS	Reynolds-averaged Navier–Stokes
2D	two-dimensional

Upper-case roman

C_p	pressure coefficient
$\overline{D}_h$	high frequency directivity function
E	spectral distribution of turbulent energy
F	switch mechanism function
G_4	function to determine the peak level of the spectrum
G_5	function to define the shape of the spectrum
H	Heaviside function
$\vec{G}_{\text{Source}}$	source vector
$\vec{G}_{\text{Trans}}$	transport vector
M	Mach number
Re	Reynolds number
St'''	Strouhal number defined as $St''' = fh/U$
U	mean velocity

Lower-case roman

c	chord length
f	defined surface, frequency
h	trailing edge thickness
i	number of grid-line
$i\kappa$	wavenumber
k	turbulent kinetic energy
l	wavelength of the energy mode
l_i	component of local force on the surface
p	pressure
p'	pressure fluctuation
p'_T	pressure fluctuation for thickness noise
p'	pressure fluctuation for loading noise
r	distance
t	time
u_x	x-component of the instantaneous velocity
u, v, w	velocity components
v_n	local normal velocity of the body
x, y, z	Cartesian coordinates

Upper-case Greek

Θ_e	angle from source streamwise axis x to observer
Φ_e	angle from source lateral axis y to observer
Ψ	solid angle
Ω	vorticity magnitude

Lower-case Greek

δ	Dirac delta function
δ^*_{avg}	average boundary layer displacement thickness
ε	turbulent dissipation rate
η	Kolmogorov scale
κ	wave number of Fourier energy mode
ν	eddy viscosity
ρ	density
ω	turbulent kinetic energy

Symbols and indices

M_n	dot product with the unit normal vector
M_r	dot product with the unit radiation vector
$\dot{M}$	source time derivative
$u_i'^*$	scaled fluctuation u' unscaled fluctuation
$\langle u_i u_i \rangle$	normal statistic fluctuation
$\phi'_i(t)$	coefficient of a constrained random process

References

[1] Ashwill T, Laird D. Concepts to facilitate very large blades. In: Proceedings of ASME/AIAA wind energy symposium 2007. Reno, NV.
[2] Oertel Jr H. Wakes behind blunt bodies. Ann Rev Fluid Mech 1990;22:539–64.
[3] Davidson L, Peng SH. Hybrid LES-RANS modeling: a one-equation SGS model combined with a k-ω model for predicting recirculating flows. International Journal for Numerical Methods in Fluids 2003;43:1003–18.
[4] Hanjalic K, Hadzabdic M, Temmerman L, Leschziner M. Merging LES and RANS strategies: zonal or seamless coupling? Direct Large Eddy Simul V 2004;5:451–64.
[5] Temmerman L, Hadzabdic M, Leschziner M, Hanjalic K. A hybrid two-layer URANS-LES approach for large eddy simulation at high Reynolds numbers. Int J Heat Fluid Flow 2005;26:173–90.
[6] Abe K, Ohtsuka T. An investigation of LES and hybrid RANS-LES models for predicting 3-D diffuser flow. International Journal of Heat and Fluid Flow 2010;31:833–44.
[7] Fröhlich J, von Terzi D. Hybrid RANS-LES methods for the simulation of turbulent flows. Prog Aero Sci 2008;44:349–77.
[8] Kim T, Lee S, Kim H, Lee S. Design of low noise airfoil with high aerodynamic performance for use on small wind turbines. Sci China 2010;53:75–9.
[9] Göçmen T, Özerdem B. Airfoil optimization for noise emission problem and aerodynamic performance criterion on small scale wind turbines. Energy 2012;46:62–71.
[10] Oerlemans S, Sijtsma P, Mendez López B. Location and quantification of noise sources on a wind turbine. J Sound Vib 2007;299:869–83.
[11] Brooks TF, Pope DS, Marcolini MA. Airfoil self-noise and prediction. NASA Reference Publication 1218; 1989.
[12] Ffowcs Williams JE, Hawkings DL. Sound generated by turbulence and surfaces in arbitrary motion. Philosophical Transactions of the Royal Society A: Mathematical, Physical & Engineering Sciences 1969;264(1151):321–42.
[13] ANSYS FLUENT 13.0 documentation. ANSYS, Inc.
[14] Amiet RK. Acoustic radiation from an airfoil in a turbulent stream. J Sound Vib 1975;41(4):407–20.
[15] Mathey F, Coklijat D, Bertoglio JP, Sergent E. Specification of LES inlet boundary condition using vortex method. In: 4th international symposium on turbulence, heat and mass transfer. Antalya, Turkey: Begell House; 2003.
[16] Tabor GR, Baba-Ahmadi MH. Inlet conditions for large eddy simulation: a review. Comput Fluids 2010;39:553–67.
[17] Lighthill MJ. On sound generated aerodynamically. I: general theory. Proceedings of the Royal Society A 1952;211:564–87.
[18] Farassat F, Succi GP. The prediction of helicopter discrete frequency noise. Vertica 1983;7(4):309–20.

[19] Brentner KS. Prediction of helicopter discrete frequency rotor noise-a computer program incorporating realistic blade motions and advanced acoustic formulation. NASA; October 1986. TM 87721.
[20] Barone M, Paquette J. Aeroacoustics and aerodynamic performance of a rotor with flatback airfoils. In: European wind energy conference 2010. Warsaw, Poland.
[21] Berg DE, Zayas JR. Aerodynamic and aeroacoustic properties of flatback airfoils. In: 46th AIAA aerospace sciences meeting and exhibit January 2008. Reno, Nevada.
[22] Migliore P, Oerlemans S. Wind tunnel aeroacoustic tests of six airfoils for use on small wind turbines; 2003. NREL/CP-5–35090.
[23] Drela M. XFOIL: an analysis and design system for low Reynolds number airfoils. In: Mueller TJ, editor. Low Reynolds number aerodynamics, lecture notes in engineering. New York: Springer; 1989. p. 54–61.
[24] Blake WK. Mechanics of flow-induced sound and vibration. Orlando, Florida, USA: Academic Press, Inc; 1986.